

Homogeneity Tests of Covariance and Change-Points Identification for High-Dimensional Functional Data

Shawn Santo*

Department of Statistical Science, Duke University,

and

Ping-Shou Zhong†

Department of Mathematics, Statistics, and Computer Science,

University of Illinois at Chicago

Abstract

We consider inference problems for high-dimensional functional data with a dense number (T) of repeated measurements taken for a large number of p variables from a small number of n experimental units. The spatial and temporal dependence, high dimensionality, and the dense number of repeated measurements all make theoretical studies and computation challenging. This paper has two aims; our first aim is to solve the theoretical and computational challenges in detecting and identifying change points among covariance matrices from high-dimensional functional data. The second aim is to provide computationally efficient and tuning-free tools with a guaranteed stochastic error control. The change point detection procedure is developed in the form of testing the homogeneity of covariance matrices. The weak convergence of the stochastic process formed by the test statistics is established under the “large p , large T and small n ” setting. Under a mild set of conditions, our change point identification estimator is proven to be consistent for change points at any location of a sequence. Its rate of convergence is shown to depend on the data dimension, sample size, number of repeated measurements, and signal-to-noise ratio. We also show that our proposed computation algorithms can significantly reduce the computation time and are applicable to real-world data with a large number of high-dimensional repeated measurements (e.g. fMRI data). Simulation results demonstrate both finite sample performance and computational effectiveness of our proposed procedures. We observe that the empirical size of the test is well controlled at the nominal level, and the locations of multiple change points can accurately be identified. An application to fMRI data demonstrates that our proposed methods can identify event boundaries in the preface of the movie *Sherlock*. Our proposed procedures are implemented in an R package *TechPhD*.

Keywords: Change points, Covariance matrix, Event segmentation, High-dimensional functional data, Spatial and temporal dependence

*Shawn Santo is an Assistant Professor of the Practice, Department of Statistical Science, Duke University, Durham, NC 27708 (e-mail: shawn.santo@duke.edu).

†Ping-Shou Zhong is an Associate Professor, Department of Mathematics, Statistics, and Computer Science, University of Illinois at Chicago, Chicago, IL 60607 (e-mail: pszhong@uic.edu).

1 Introduction

The covariance matrix or precision matrix, defined as the inverse of the covariance matrix, is very commonly used in applications to characterize dependence. For example, in fMRI studies the covariance matrix is often used to quantify relationships between spatially separated brain regions. Neuroscientists and statisticians use these relationships to better understand the brain’s functional connectivity. Our work is motivated by an experiment conducted by Chen et al. (2017), where 17 participants watched the same 48-minute segment of the BBC television series *Sherlock*. The study cultivated blood-oxygen-level dependent (BOLD) readings in spatially separated brain regions for all subjects. The goal of the experiment was to understand perception and memory processes in humans as they experience continuous real-world events, such as watching a movie. Event segmentation theory, posited by Zacks et al. (2007), suggests that humans may partition a continuous experience into a series of segmented discrete events for memory storage. Schapiro et al. (2013) has suggested that these event boundaries from the partitions are created around changes in functional connectivity. Identifying change points with regards to functional connectivity via the covariance matrix provides an objective and meaningful approach to discover event boundaries. This fosters our understand of how subjects processed the continuous stream of audio and visual stimuli exposed to them during their viewing of *Sherlock*.

Assume $Y_{it} = (Y_{it1}, \dots, Y_{itp})^T$ is a p -dimensional random vector with mean vector μ_t and covariance matrix Σ_t . In a typical fMRI study at the voxel level, Y_{it} ($i = 1, \dots, n$; $t = 1, \dots, T$) represents the p BOLD signal measurements for the i -th individual observed at the t -th time point, where p , T , and n are at the order of 100,000, 100, and 10, respectively. For the region of interest (ROI) analysis, p represents the number of spatially separated brain regions and is at the order of 100. We are dealing with a high dimensional functional data setting where the dimension of functional curves (p) are comparable or far exceeds T and n . This setting is different from the classical multivariate functional data setting where p is fixed and does not grow with n and T . (e.g., Chiou et al, 2014). The goal of this paper is to develop nonparametric, computationally efficient and tuning-free statistical procedures to detect and identify change points among covariance matrices in high-dimensional functional

data with a dense number of repeated measurements (Li and Hsing, 2010). The covariance change point detection problem can be posed in the form of a statistical hypothesis test as

$$\begin{aligned} H_0 : \Sigma_1 = \cdots = \Sigma_T = \Sigma \quad & \text{versus} \\ H_1 : \Sigma_1 = \cdots = \Sigma_{\tau_1} \neq \Sigma_{\tau_1+1} = \cdots = \Sigma_{\tau_q} \neq \Sigma_{\tau_q+1} = \cdots = \Sigma_T, \end{aligned} \quad (1)$$

where $\tau_k < T$ ($k = 1, \dots, q < \infty$) are the unknown change point locations. If we reject stationarity among Σ_t , the second task is to estimate the unknown locations of change points τ_k s.

In functional data literature, Y_{it} is considered as a realization of p -dimension functional curves measured with errors observed at time t . Many recently developed inference methods for low-dimensional (small p) functional data are summarized in Horváth and Kokoszka (2012). Most inference methods designed for the low-dimensional cases can not be applied to our setting because they depend on functional principal components analysis (FPCA) in the final implementation (Horváth and Kokoszka, 2012; Hall et al., 2006). FPCA has been demonstrated to not be reliable for high-dimensional functional data. One reason is that the smoothing and PCA steps are very computationally expensive, if not infeasible, due to the high dimensionality and the large number of repeated measurements of Y_{it} (Xiao et al., 2016). Second, PCA is not consistent when the data dimension p is larger than n (Jung and Marron, 2009). To overcome these difficulties, we develop a new statistical inference approach for high-dimensional functional data. Our approach avoids the smoothing and FPCA steps and provides a computationally efficient and statistically rigorous approach for high-dimensional functional data. Although we consider a high-dimensional setting, we do not require a sparsity assumption for Σ_t , which is commonly used in high-dimensional covariance or precision matrix estimation literature (e.g., Bickel and Levina, 2008; Pourahmadi, 2013). In addition, we admit a general spatiotemporal dependence structure in $\{Y_{it}\}_{t=1}^T$, and stationarity in temporal dependence among $\{Y_{it}\}_{t=1}^T$ is not required. Stationarity implies that the temporal dependence between Y_{it} and Y_{is} is the same as that between Y_{iu} and Y_{iv} if $t - s = u - v \neq 0$.

The hypothesis test considered in (1) is also related but significantly different from homogeneity tests of covariance matrices in multivariate statistical analysis. For low dimensional

data with a fixed data dimension p , Anderson (2003) and Muirhead (2005) detailed the classical likelihood ratio tests. However, the likelihood ratio tests require n to exceed p and are only applicable to temporally independent samples. The multivariate tests for the homogeneity of high-dimensional covariance matrices have received much attention in the past few years. A partial list includes Schott (2007), Srivastava and Yanagihara (2010), Li and Chen (2012), Zhang et al. (2018) and Ishii et al. (2016, 2019). Most of the existing research developed tests under a temporal independence assumption except for Zhong et al. (2019) who considered high-dimensional longitudinal data with T fixed and small. All existing methods considered an asymptotic setting with a fixed number of groups or repeated measurements (i.e., T is fixed and small). It is worthwhile to emphasize that extending finite T results to diverging T is challenging both theoretically and computationally.

Our proposed methods are naturally connected to covariance change point literature. In addition to a change point detection method, we propose a method to estimate unknown locations of change points. Much of the research in high-dimensional covariance change point identification considers the scenario with temporal independent samples. For instance, Wang et al. (2017) considered covariance matrix change point identification for T independent p -dimensional sub-Gaussian random vectors which requires $p < T$. Dette et al. (2018) proposed a two-stage covariance change point identification procedure based on T independent sub-Gaussian random vectors. In stage one their procedure involved dimension reduction governed by a regularization parameter. In stage two they used a CUSUM-type statistic to estimate the locations of change points. Despite these recent advances, none of the aforementioned change point identification methods are applicable to high-dimensional functional data. We study the rate of convergence of the proposed change point estimator under an asymptotic setting that is suitable for high-dimensional dense functional data where p , n , and T all diverge, but we do not require restrictive conditions on the relationships between p , n and T . Our proposed method is able to consistently estimate change points τ_k that occur at any location in a sequence such that $\tau_k \asymp T^{\delta_k}$ for some $0 \leq \delta_k \leq 1$. This is more broader than the typical assumption of $\tau_k \asymp T$ in the existing literature.

This paper provides both theoretical and computational contributions. From a theoretical perspective, we investigate covariance tests and change point identification for high-

dimensional functional data, under a setting in which n , p , and T diverge. For T diverging, the test statistic forms a stochastic process. The convergence of the finite- T distributions (e.g., Zhong et al., 2019) is not sufficient for weak convergence of a stochastic process with diverging T . In addition, the complex temporal and spatial dependence must be carefully addressed. Thus, it is non-trivial to establish weak convergence of our proposed test statistic. We also discover a parameter-free asymptotic distribution under the temporal stationary assumption, which makes a connection with the classical literature. Furthermore, we derive the rate of convergence for the change point estimator for change points at any location in the sequence. Our investigation reveals that the rate of convergence depends on the data dimension, sample size, number of repeated measurements, and signal-to-noise ratio. The change point identification estimator is shown to be consistent, even for the change points that are close to the boundaries, provided the signal strength exceeds the noise. To the best of our knowledge, the asymptotic framework in which n , p , and T all diverge has not previously been investigated with regards to change point identification among high-dimensional covariance matrices.

From a computational perspective, we develop an efficient algorithm for our methods, and thus make it practical to apply our procedure to fMRI data sets and others with similar structure. We introduce two recursive relationships and computation efficient formulae as a way to reduce the computation complexity from $O(pn^4T^6)$ to $O(pn^2T^4)$. A quantile approximation technique is shown to further decrease the complexity to the order of pn^2T^3 . The approximation technique’s accuracy is demonstrated through simulation studies. These improvements are included in an R package, *TechPhD*, an abbreviation of “Tests and Estimation of Covariance cHange-Points for High-dimensional Data” which provides an option for parallel computing.

From a practical point of view, our proposed method is attractive because it is free of tuning parameters, and has a guaranteed stochastic error control under very general assumptions. Researchers in neuroscience have developed various methods to study dynamic functional brain connectivity for single patients and populations. Most of the existing work studies dynamic functional connectivity using a sliding window approach (e.g., Monti et al., 2014) or regularization approach (e.g., Kundu et al., 2018) by directly estimating the

locations of change points without detecting the existence of change points. Both of the aforementioned approaches depend on tuning parameters; these are often difficult to select in practice. In general, these change point identification methods developed in neuroscience are ad hoc and lack the theoretical rigor to ensure a consistent and robust procedure. Our proposed procedure is free of tuning parameters and is theoretically rigorous. There do exist some resampling methods for detecting the existence of change points. However, most of these methods assume temporal independence or stationary temporal dependence with a specific structure. For example, vector autoregressive models are applied in Barnett and Onnela (2016) and Zalesky et al. (2014), and strict stationarity was used in the bootstrap procedure proposed in Cribben et al. (2013).

The remaining sections of this paper are organized as follows. Section 2 details the statistical model and our basic setting. Section 3 introduces our proposed test procedures. The test statistic’s asymptotic distribution is derived under the asymptotic framework in which n , p , and T diverge. Computation consideration with regards to the test procedure is provided in Section 4. Section 5 introduces an estimator to identify the locations of change points should we reject H_0 of (1). The estimator’s rate of convergence is studied, and a binary segmentation procedure is detailed to estimate the locations of multiple change points. Sections 6 and 7 demonstrate the finite sample performance via simulation and an application to event segmentation through the motivating example, respectively. All proofs and technical details are provided in the Supplementary material.

2. Data model and basic setting

Suppose we have n independent individuals that have p variables recorded at each of T identical time points. Let $Y_{it} = (Y_{it1}, \dots, Y_{itp})^T$ be an observed p -dimensional random vector, where Y_{it} ($i = 1, \dots, n$; $t = 1, \dots, T$) is independently and identically distributed for all n individuals. Assume Y_{it} follows a general factor model, where

$$Y_{it} = \mu_t + \Gamma_t Z_i, \tag{2}$$

and μ_t is a p -dimensional unknown mean vector, Γ_t is an unknown $p \times m$ matrix such that $m \geq pT$, and Z_i ’s are independent m -dimensional multivariate standard normal random

vectors. Since $\text{var}(Z_i) = I_m$, it follows that for the i th individual, $\text{cov}(\Gamma_s Z_i, \Gamma_t Z_i) = \Gamma_s \Gamma_t^T$. We define $\Gamma_s \Gamma_t^T$ as C_{st} for different time points, s and t , and define $\Gamma_t \Gamma_t^T$ as Σ_t . Thus, for the i th individual, $\text{cov}(Y_{is}, Y_{it}) = C_{st}$ if $s \neq t$ and $\text{cov}(Y_{is}, Y_{it}) = \Sigma_t$ if $s = t$ for all $s, t \in \{1, \dots, T\}$. For individuals $i \neq j$, $\text{cov}(Y_{is}, Y_{jt}) = 0$. By definition, C_{st} and Σ_t are $p \times p$ matrices for all $s, t \in \{1, \dots, T\}$. No specific structure is required on covariance matrices C_{st} and Σ_t . Their generality allows us to capture the spatiotemporal dependence in and among the random vectors Y_{it} ($i = 1, \dots, n$; $t = 1, \dots, T$). In the context of fMRI data, spatial dependence is present among neighboring voxels or nodes and is captured in both C_{st} and Σ_t . Temporal dependence exists for the same voxel or node across time points and is captured in matrix C_{st} .

The factor model in (2) includes the commonly used models (e.g., Horváth and Kokoszka, 2012; Li and Hsing, 2010) in functional data literature as a special case where Y_{it} is assumed to be generated from the following model:

$$Y_{it} = \mu_t + X_i(t) + \varepsilon_{it}, \quad (3)$$

where $X_i(t)$ is a Gaussian process with mean 0 and covariance function $\text{cov}\{X_i(t), X_i(s)\} = C_x(t, s)$ and ε_{it} are independent normally distributed nugget effects with variance $\text{var}(\varepsilon_{it}) = \sigma^2 I_p$. Under the model (3), the null hypothesis in (1) is equivalent to test the equivalence of the covariances $C_x(t, t)$ for $t = 1, \dots, T$. The model (3) is a special case of model (2), by defining $\Gamma = (\Gamma_1^T, \dots, \Gamma_T^T)^T = (C_x + \sigma^2 I_{pT})^{1/2}$ where $C_x = \{C_x(i, j)\}_{i,j=1}^T$ is a $pT \times pT$ -dim matrix.

3. Homogeneity tests of covariance matrices

To avoid the inconsistency and uncertainty due to the dimension reduction methods as in functional PCA, our proposed method directly solves the testing problem by considering a measure to quantify the differences among the high-dimensional covariances Σ_t 's. We use D_t ($t = 1, \dots, T-1$) to measure the averaged distance of the covariance matrices before and after time t , where

$$D_t = \frac{1}{w(t)} \sum_{s_1=1}^t \sum_{s_2=t+1}^T \text{tr}\{(\Sigma_{s_1} - \Sigma_{s_2})^2\}, \quad (4)$$

and $w(t) = t(T-t)$. Let $\mathcal{T} = \{1, \dots, T-1\}$. The choice of D_t is motivated by the fact that we can distinguish between H_0 and H_1 based on the maximum value of D_t for all $t \in \mathcal{T}$. Under H_0 of (1), $\max_{t \in \mathcal{T}} D_t = 0$, and under H_1 , $\max_{t \in \mathcal{T}} D_t > 0$. Moreover, consider redefining the domain of the function $\text{tr}\{(\Sigma_{s_1} - \Sigma_{s_2})^2\}$ on $\{s_1, s_2\} \in \mathcal{T} \times \mathcal{T}$ as a function $\text{tr}\{(\Sigma_{u_1} - \Sigma_{u_2})^2\}$ on $\{u_1, u_2\} \in \mathcal{U} \times \mathcal{U}$ where $\mathcal{U} = \{1/T, \dots, 1 - 1/T\}$. Then, D_t is a discretized approximation of $D(u) = \int_0^u \int_u^1 \text{tr}\{(\Sigma_{u_1} - \Sigma_{u_2})^2\} du_1 du_2$ for $u = t/T$. Although jump changes exist among the covariance matrices Σ_t (or Σ_u) under H_1 , $D(u)$ is still a continuous function on $[0, 1]$. The continuity property of $D(u)$ can be utilized to simplify the computation complexity, which will be discussed in detail in Section 4.

A linear combination of U-statistic estimators is used to create an unbiased estimator of D_t . Our test statistic is constructed in the same manner as those in Zhong et al. (2019). Let $P_n^k = n!/(n-k)!$ and let $\tilde{\sum}$ summation notation represent the summation over mutually different indices. For example, $\tilde{\sum}_{i,j,k}$ means that the summation over i, j , and k is defined such that $i \neq j$, $j \neq k$, and $k \neq i$. Let $U_0(s, t, q, r) = \tilde{\sum}_{i,j} Y_{is}^T Y_{jt} Y_{iq}^T Y_{jr} / P_n^2$, $U_1(s, t, q, r) = \tilde{\sum}_{i,j,k} Y_{is}^T Y_{jt} Y_{iq}^T Y_{kr} / P_n^3$ and $U_2(s, t, q, r) = \tilde{\sum}_{i,j,k,l} Y_{is}^T Y_{jt} Y_{kq}^T Y_{lr} / P_n^4$ be unbiased estimators of $\text{tr}\{(C_{rt} + \mu_r \mu_t^T)(C_{sq} + \mu_s \mu_q^T)\}$, $\text{tr}\{(C_{sq} + \mu_s \mu_q^T) \mu_r \mu_t^T\}$ and $\text{tr}(\mu_s \mu_q^T \mu_r \mu_t^T)$, respectively. Then, $U(s, t, q, r) = U_0(s, t, q, r) - U_1(s, t, q, r) - U_1(t, s, r, q) + U_2(s, t, q, r)$ is an unbiased estimator of $\text{tr}(C_{sq} C_{tr}^T)$. The distance measure, D_t , can be expressed as $D_t = w^{-1}(t) \sum_{s_1=1}^t \sum_{s_2=t+1}^T \{\text{tr}(\Sigma_{s_1}^2) + \text{tr}(\Sigma_{s_2}^2) - \text{tr}(\Sigma_{s_1} \Sigma_{s_2}) - \text{tr}(\Sigma_{s_2} \Sigma_{s_1})\}$. To simplify notation, denote $U(s_1, s_2, s_1, s_2)$ as $U_{s_1 s_2}$. An unbiased estimator of $\text{tr}(\Sigma_{s_1} \Sigma_{s_2})$ is given by $U_{s_1 s_2}$ which is

$$U_{s_1 s_2} = U_0(s_1, s_2, s_1, s_2) - U_1(s_1, s_2, s_1, s_2) - U_1(s_2, s_1, s_2, s_1) + U_2(s_1, s_2, s_1, s_2). \quad (5)$$

Therefore, an unbiased estimator of D_t is

$$\hat{D}_{nt} = \frac{1}{w(t)} \sum_{s_1=1}^t \sum_{s_2=t+1}^T \sum_{a,b=1}^2 (-1)^{|a-b|} U_{s_a s_b}. \quad (6)$$

The leading order variance of \hat{D}_{nt} is $\text{var}(\hat{D}_{nt}) = \sigma_{nt}^2 \{1 + o(1)\}$, where $\sigma_{nt}^2 = w^{-2}(t)(4V_{0t}/n^2 +$

$8V_{1t}/n$), and

$$V_{0t} = \sum_{\substack{s_1, s_2, \\ h_1, h_2}}^* \sum_{\substack{u, v, \\ k, l \in \{1, 2\}}} (-1)^{|u-v|+|k-l|} \text{tr}^2(C_{s_u h_k} C_{s_v h_l}^T), \quad (7)$$

$$V_{1t} = \sum_{\substack{s_1, s_2, \\ h_1, h_2}}^* \sum_{u, k \in \{1, 2\}} (-1)^{|u-k|} \text{tr}\{(\Sigma_{s_1} - \Sigma_{s_2}) C_{s_u h_k} (\Sigma_{h_1} - \Sigma_{h_2}) C_{s_u h_k}^T\}. \quad (8)$$

Notation $\sum_{\substack{s_1, s_2, \\ h_1, h_2}}^*$ present in equations V_{0t} and V_{1t} is defined as $\sum_{s_1=1}^t \sum_{s_2=t+1}^T \sum_{h_1=1}^t \sum_{h_2=t+1}^T$.

We consider an asymptotic framework where $p(n) \rightarrow \infty$ and $T(n) \rightarrow \infty$ as $n \rightarrow \infty$, where p and T are both functions of n . A specific functional form is not required, and we do not require any specific growth rate relationships between p , T , and n . This makes our asymptotic results applicable to many scenarios such as $p > n$ and $p > T$, or $p > n$ and $T > p$. To establish the limiting distribution of \hat{D}_{nt} , we assume Conditions C1 - C4. From C4, $f(s) \asymp g(s)$ means that $f(s)$ and $g(s)$ are of the same order. Thus, $f(s) \asymp g(s)$ implies there exist constants c_1 and c_2 such that $|f(s)| \leq c_1 |g(s)|$ and $|g(s)| \leq c_2 |f(s)|$ for every s . Define $A^{\otimes 2} = AA^T$.

C1. $\text{tr}\{(\Gamma_{s_2}^T C_{s_1 h_1} \Gamma_{h_2})^{\otimes 2}\} = o(V_{0t})$ for any $s_1, s_2, h_1, h_2 \in \{1, \dots, T\}$.

C2. $\text{tr}[\{(\Gamma_{s_1} + \Gamma_{s_2})^T (\Sigma_{s_1} - \Sigma_{s_2}) (\Gamma_{s_1} - \Gamma_{s_2})\}^{\otimes 2}] = o(nV_{1t})$ for $s_1 \in \{1, \dots, t\}$ and $s_2 \in \{t+1, \dots, T\}$.

C3. $\sum_{\substack{s_1, s_2, \\ h_1, h_2}}^* \text{tr}^4(C_{s_u h_k} C_{s_v h_l}^T) = o(V_{0t}^2)$, for any $u, k, v, l \in \{1, 2\}$.

C4. There exists a function $\psi(k)$ such that $\psi(k) > 0$ and $\sum_{k=1}^{\infty} \psi^{1/2}(k) < \infty$. For any $s_1, s_2 \in \{1, \dots, T\}$, $\text{tr}^2(C_{s_1 s_2} C_{s_1 s_2}^T) \asymp \psi(|s_1 - s_2|) \text{tr}^2(\Sigma_{s_1} \Sigma_{s_2})$.

If all eigenvalues of Σ_t are bounded and the temporal dependence is not too strong, then Condition C1 holds. Condition C2 is not needed under the null hypothesis. Condition C3 is a mild condition. Consider the setting when no temporal dependence exists, then $V_{0t} = \sum_{s_1=1}^t \sum_{s_2=t+1}^T \sum_{u, v \in \{1, 2\}} \text{tr}^2(\Sigma_{s_u} \Sigma_{s_v})$. Similarly, the left-hand side of Condition C3 is $\sum_{s_1=1}^t \sum_{s_2=t+1}^T \sum_{u, v \in \{1, 2\}} \text{tr}^4(\Sigma_{s_u} \Sigma_{s_v})$. Furthermore, if all eigenvalues of Σ_t are bounded for all $t \in \{1, \dots, T\}$, then $V_{0t}^2 \asymp \{t(T-t)p^2\}^2$. The left-hand side of Condition C3 is of the order $t(T-t)p^4$. As a result, Condition C3 holds. Condition C4 imposes mild requirements on the spatiotemporal structure.

The below theorem establishes the asymptotic distribution of \hat{D}_{nt} .

Theorem 1. *Under Conditions C1 – C3, for any fixed t , as $n \rightarrow \infty$,*

$$\sigma_{nt}^{-1}(\hat{D}_{nt} - D_t) \xrightarrow{d} N(0, 1),$$

where $\sigma_{nt}^2 = w^{-2}(t)(4V_{0t}/n^2 + 8V_{1t}/n)$ and V_{0t} and V_{1t} are given in (7) and (8), respectively.

Under the null hypothesis, it follows that $\sigma_{nt,0}^{-1}\hat{D}_{nt} \rightarrow N(0, 1)$ in distribution, where $\sigma_{nt,0}^2 = w^{-2}(t)(4V_{0t}/n^2)$ and only Conditions C1 and C3 are required. To formulate an appropriate test procedure free of tuning parameters, consider the test statistic \mathcal{M}_n , where

$$\mathcal{M}_n = \max_{t \in \mathcal{T}} \hat{\sigma}_{nt,0}^{-1} \hat{D}_{nt}, \quad (9)$$

and $\hat{\sigma}_{nt,0}^2 = 4\hat{V}_{0t}/\{nw(t)\}^2$. Estimator \hat{V}_{0t} can be constructed by replacing $\text{tr}(C_{s_u h_k} C_{s_v h_l}^T)$ in V_{0t} by $U(s_u, s_v, h_k, h_l)$.

Let $R_{n,z}$ be a correlation matrix with (t, q) component defined as $R_{n,tq} = \text{corr}(\hat{D}_{nt}, \hat{D}_{nq})$. We assume that as $n \rightarrow \infty$, $R_{n,z}$ converges to R_z . Specifically, the leading order of the $\text{cov}(\hat{D}_{nt}, \hat{D}_{nq})$ is $w^{-1}(t)w^{-1}(q)(4V_{0,tq}/n^2)$, where

$$V_{0,tq} = \sum_{s_1=1}^t \sum_{s_2=t+1}^T \sum_{h_1=1}^q \sum_{h_2=q+1}^T \sum_{\substack{u,v, \\ k,l \in \{1,2\}}} (-1)^{|u-v|+|k-l|} \text{tr}^2(C_{s_u h_k} C_{s_v h_l}^T). \quad (10)$$

Thus, $R_{n,tq} = V_{0,tq}/(V_{0,t}V_{0,q})^{1/2}$. The following theorem establishes the asymptotic distribution of \mathcal{M}_n , where n , p , and T all diverge.

Theorem 2. *Under Conditions C1, C3, and C4, H_0 of (1), and as $n \rightarrow \infty$, \mathcal{M}_n has the same limiting distribution as $\max_{t \in \mathcal{T}} Z_t$, where Z_t is a Gaussian process with mean 0 and covariance R_z .*

Theorem 2 presents the asymptotic distribution of \mathcal{M}_n under general conditions. Let $W = \max_{t \in \mathcal{T}} Z_t$, where Z_t is a Gaussian process with mean 0 and covariance R_z . Define W_α as the quantile such that $\text{pr}(W > W_\alpha) = \alpha$. By Theorem 2, \mathcal{M}_n converges to W in distribution, and an α -level test rejects the null hypothesis in (1) if $\mathcal{M}_n > W_\alpha$.

An estimate of W_α depends on quantity $R_{n,z}$. Therefore, we consider an estimator for $V_{0,tq}$, given by $\hat{V}_{0,tq}$, which replaces $\text{tr}(C_{s_u h_k} C_{s_v h_l}^T)$ by $U(s_u, s_v, h_k, h_l)$. Let $\hat{R}_{n,tq} = \hat{V}_{0,tq}/\{\hat{V}_{0,t}\hat{V}_{0,q}\}^{1/2}$ be an estimator for $R_{n,tq}$. However, this method is not computationally

efficient because the random variable W depends on R_z , a $(T-1) \times (T-1)$ matrix, and one need to compute $\hat{R}_{n,tq}$ for each $t, q \in \{1, \dots, T-1\}$. A direct computation is very challenging because the computation complexity of this approach, in terms of T , is at the order of T^4 for each component. Therefore, total complexity (in terms of T) is at the order of T^6 to compute $\hat{R}_{n,z}$. As a result, it is computationally inefficient to compute all components of $\hat{R}_{n,z}$ exactly when T is large. This lead us to carefully consider a set of recursive formulae and an approximation procedure in detailed in Section 4. These methods are shown to improve computation efficiency while maintaining accuracy.

In some special cases, the asymptotic distribution in Theorem 2 can be simplified. In the following corollary, we consider two important special cases: temporal independence and temporal stationary. Assume that temporal stationary so that $C_{st} = C_{uv}$ for any $s - t = u - v \neq 0$, and correspondingly, define $C(d) = C_{st}$ for $s - t = d > 0$. The temporal independent case is a special case of temporal stationary with $C(d) = 0$ for $d > 0$. The technical conditions in C1, C3 and C4 can be simplified and reduced to the following two conditions:

C1'. $\text{tr}\{(C(d)\Sigma C^T(d)\Sigma)\} = o\{T^3\text{tr}^2(\Sigma^2)\}$ for any $d \in \{1, \dots, T-1\}$.

C4'. There exists a function $\psi(k)$ such that $\psi(k) > 0$ and $\sum_{k=1}^{\infty} \psi^{1/2}(k) < \infty$. For any $d \in \{1, \dots, T-1\}$, $\text{tr}^2\{C(d)C^T(d)\} \asymp \psi(d)\text{tr}^2(\Sigma^2)$.

Corollary 1. *Assume that temporal stationary holds and $t/T \rightarrow \lambda$ as $T \rightarrow \infty$ for $0 \leq \lambda \leq 1$. Under Conditions C1', C4' and H_0 , $\hat{\sigma}_{nt,0}^{-1}\hat{D}_{nt}$ converges to a Gaussian process with representation $Z(\lambda) = \{(1-\lambda)W(\lambda) + \lambda(W(1) - W(\lambda))\}/\sqrt{\lambda(1-\lambda)}$, where $W(\lambda)$ is a standard Brownian motion.*

This result in Corollary 1 may be considered as an extension of Dehling et al. (2013) to high-dimensional functional data. Under conditions in Corollary 1,

$$\sigma_{nt,0}^2 = 4T^3(1-\lambda)\lambda\sigma_0^2[\text{tr}^2(\Sigma^2) + \sum_{d=1}^{\infty} \text{tr}^2\{C(d)C^T(d)\}]/\{nw(t)\}^2.$$

Thus, the computational cost can be significantly reduced because we do not need to compute the correlation matrix $\hat{R}_{n,z}$ in Theorem 2, and the estimation of $\sigma_{nt,0}^2$ is not computationally

difficult. However, the results in Corollary 1 is not generally true for a temporal non-stationary data. Thus, we will consider the computational issues for general case in the next section.

4. Computation methods and approximations

If a direct computation approach is taken, then the overall computation complexity for the change point detection procedure in Section 3 is at the order of pn^4T^6 . This is impracticable for data sets with large n and T . We introduce multiple methods to reduce this complexity through recursive formulae and lightweight approximations.

Consider the computation complexity with respect to the sample size n . For given quantities s, t, q, r , if a direct computation is utilized, the computation complexity of $U(s, t, q, r)$ is at the order of n^4 . This is from term $U_2(s, t, q, r)$ that has computation complexity at the order of n^4 . In addition, term $U_1(s, t, q, r)$ has computation complexity at the order of n^3 . To save computation cost, we can rewrite $U_1(s, t, q, r)$ and $U_2(s, t, q, r)$ in a computation efficient form as follows. Consider $U_1(s, t, q, r)$, which can be rewritten as

$$\begin{aligned} P_n^3 U_1(s, t, q, r) = & \sum_{i=1}^n \left(\sum_{j=1}^n Y_{is}^T Y_{jt} \right) \left(\sum_{k=1}^n Y_{iq}^T Y_{kr} \right) - \sum_{i=1}^n \sum_{j=1}^n Y_{is}^T Y_{jt} Y_{iq}^T Y_{jr} \\ & - \sum_{i=1}^n \sum_{k=1}^n Y_{is}^T Y_{it} Y_{iq}^T Y_{kr} - \sum_{i=1}^n \sum_{j=1}^n Y_{is}^T Y_{jt} Y_{iq}^T Y_{jr}. \end{aligned} \quad (11)$$

The first term in expression (11), has computation complexity at the order of $2n^2$. Therefore, the computation complexity of $U_1(s, t, q, r)$ regarding the sample subjects is at the order of n^2 , not n^3 . Quantity $U_{s_1 s_2, 2}$ can be written as

$$\begin{aligned} P_n^4 U_2(s, t, q, r) = & \left(\sum_{i \neq j=1}^n Y_{is}^T Y_{jt} \right) \left(\sum_{k \neq l=1}^n Y_{kq}^T Y_{lr} \right) - P_n^3 \{U_1(s, t, q, r) + U_1(s, t, r, q) \\ & + U_1(t, s, q, r) + U_1(t, s, r, q)\} - P_n^2 \{U_0(s, t, q, r) + U_0(s, t, r, q)\}. \end{aligned} \quad (12)$$

Based on the above expression for $U_2(s, t, q, r)$, the computation complexity of $U_2(s, t, q, r)$ regarding the sample subjects can be reduced to the order of n^2 . In summary, the computation cost of statistics $U_{s_1 s_2}$ and $U(s, t, q, r)$, for fixed s, t, q, r , with regard to sample subjects is at the order of n^2 .

We now reduce the computation cost with respect to T . If a direct computation method is applied, the computation complexity of \hat{D}_{nt} in (6) in terms of T is at the order T^3 . To reduce the complexity in terms of T , we write \hat{D}_{nt} recursively. Let $f(s_1, s_2) = (U_{s_1 s_1} + U_{s_2 s_2} - U_{s_1 s_2} - U_{s_2 s_1})$ such that $s_1, s_2 \in \{1, \dots, T\}$. By definition, it follows that for $t \geq 2$,

$$\hat{D}_{nt} = \frac{w(t-1)}{w(t)} \hat{D}_{n(t-1)} - w^{-1}(t) \sum_{k=1}^{t-1} f(k, t) + w^{-1}(t) \sum_{k=t+1}^T f(t, k). \quad (13)$$

When $t = 1$ the computation complexity of \hat{D}_{n1} is at the order of T . Therefore by (13), for each $t \in \{1, \dots, T-1\}$ the computation complexity in terms of T is at the order T . Since we compute \hat{D}_{nt} for all $t \in \{1, \dots, T-1\}$, the total computation complexity in terms of T is at the order of T^2 rather than T^3 . As a result, the overall computation complexity to compute \hat{D}_{nt} for all $t \in \{1, \dots, T-1\}$ is at the order of $pn^2 T^2$. If parallel computing is available, the computation time can further be reduced.

The greatest cost in terms of computation is due to $\hat{R}_{n,tq}$ for all $t, q \in \mathcal{T}$, where the complexity is at the order of $pn^2 T^6$, provided (11) and (12) are applied. To reduce the complexity, we express $\hat{V}_{0,tq}$ recursively. Let

$$g(s_1, h_1, s_2, h_2) = \sum_{\substack{u,v, \\ k,l \in \{1,2\}}} (-1)^{|u-v|+|k-l|} U^2(s_u, s_v, h_k, h_l),$$

$$h(t, q) = \sum_{s_1=1}^t \sum_{s_2=t+1}^T \sum_{h_1=1}^q \sum_{h_2=q+1}^T g(s_1, h_1, s_2, h_2).$$

Thus, $n^2 w(t)w(q)\hat{V}_{0,tq}/4 = h(t, q)$. Suppose quantity $h(t, q-1)$ is known for $t \in \{1, \dots, T-2\}$ and $q \in \{2, \dots, T-1\}$. For a fixed t ,

$$h(t, q) = h(t, q-1) - \sum_{j=t}^{q-1} \sum_{k=t+1}^T g(t, j, k, q) + \sum_{j=t+1}^T \sum_{k=q+1}^T g(t, q, j, k). \quad (14)$$

An analogous recursive formula can be derived to traverse a fixed column where $h(t-1, q)$ is known, and we want to compute $h(t, q)$. By the definition of $\hat{V}_{0,tq}$, quantities $\hat{V}_{0,11}$, $\hat{V}_{0,1(T-1)}$, $\hat{V}_{0,(T-1)(T-1)}$ can each be computed at the computation complexity in terms of T at the order T^2 . If we only compute $\hat{V}_{0,tq}$ for t and q that are close to boundaries 1 and $T-1$, where $\min\{t, T-t\}$ and $\min\{q, T-q\}$ is finite, then the computation complexity for each $\hat{V}_{0,tq}$ is at the order of $n^2 p T^2$. However, if t or q is not close to boundaries 1 and $T-1$, then the

computation cost for each $\hat{V}_{0,tq}$ is much larger. This motivates us to consider the following approximations.

To further reduce the computation cost, we will introduce two approximation steps for computing $\hat{R}_{n,z}$. One approximation reduces the computation costs for each term $\hat{R}_{n,tq}$ for all t or q not close to boundaries 1 and $T - 1$. Another approximation reduces the total number of $\hat{V}_{0,tq}$ to be computed.

We first consider the approximation of $\hat{R}_{n,tq}$ for t and q that are not close to the boundaries. Consider scenarios such that $t/T \rightarrow u$ and $q/T \rightarrow v$ as $T \rightarrow \infty$. Quantity $\hat{R}_{n,tq} = \hat{V}_{0,tq}/(\hat{V}_{0,t}\hat{V}_{0,q})^{1/2}$ is an approximation of $\hat{R}_n(u, v)$; this is an integration of the function $g^*(x_1, x_2, y_1, y_2) = g(s_1, h_1, s_2, h_2)$, where x_1, x_2, y_1 and y_2 are limits of $s_1/T, s_2/T, h_1/T$ and h_2/T , respectively. Let $\hat{V}_0(u, v) = \int_0^u \int_u^1 \int_0^v \int_v^1 g^*(x_1, x_2, y_1, y_2) dy_2 dy_1 dx_2 dx_1$. We can then write $\hat{R}_n(u, v)$ as

$$\hat{R}_n(u, v) = \hat{V}_0(u, v) / \{\hat{V}_0(u, u) \hat{V}_0(v, v)\}^{1/2}.$$

If T is large, $\hat{R}_{n,tq}$ is very close to $\hat{R}_n(u, v)$. We may consider $\hat{R}_n(u, v)$ as a “population” version of $\hat{R}_{n,tq}$ that we want to approximation. To reduce the computation cost, we can reduce the number of summations in approximating $\hat{R}_n(u, v)$. When T is large, instead of using all grid points $\{1, \dots, T\}$, we consider reducing the number to the order of \sqrt{T} so that the new grid points are $\mathcal{J} = \{t_1, \dots, t_J\} := \{1, J, 2J, \dots, T\}$, where $J = \lfloor \sqrt{T} \rfloor$. Term $\hat{R}_n(u, v)$ can be approximated by $\hat{R}_n(u, v) = \hat{V}_{0,u^*q^*} / \{\hat{V}_{0,u^*u^*} \hat{V}_{0,q^*q^*}\}^{1/2}$, where

$$\hat{V}_{0,u^*q^*} = \sum_{s_1=1}^{u^*} \sum_{s_2=t^*+1}^J \sum_{h_1=1}^{q^*} \sum_{h_2=q^*+1}^J g(t_{s_1}, t_{h_1}, t_{s_2}, t_{h_2}). \quad (15)$$

Let $u^* = t_u$ for $t_u \in \mathcal{J}$ such that t_u/T is closest to u , and let $q^* = t_v$ for $t_v \in \mathcal{J}$ such that t_v/T is closest v . From this approximation we can effectively reduce the computational cost for those $\hat{R}_{n,tq}$ (with t and q that are not close the boundaries) to the order of $n^2 p T^2$.

Next we consider reducing the number of $\hat{R}_{n,tq}$ terms needed to be computed. Rather than compute $\hat{R}_{n,tq}$ for all $t, q \in \{1, \dots, T - 1\}$, we can compute $h = (b + I)$ off-diagonals of the matrix and interpolate the remaining values because of the continuity of $\hat{R}_n(u, v)$ with respect to u and v . Let b be the number of consecutive off-diagonals immediately following the main diagonal, and let I be the number of off-diagonals computed at a fixed interval after the b consecutive off-diagonals. Let $\text{diag}(\hat{R}_{n,1,d+1})$ be the d th off-diagonal, where

$d \in \{1, \dots, T-2\}$. For an efficient approximation of $\hat{R}_{n,z}$, first compute $\hat{R}_{n,1,1}$. Next, apply (14) to compute $\text{diag}(\hat{R}_{n,1,2}), \dots, \text{diag}(\hat{R}_{n,1,b})$ for the corresponding b off-diagonals. Lastly, apply the formula (15) to compute $\text{diag}(\hat{R}_{n,1,I_1}), \dots, \text{diag}(\hat{R}_{n,1,I_I})$ that correspond to the I off-diagonals at a fixed interval. Each of these I off-diagonals has an initial computation in terms of T at the order T^2 . The overall complexity in terms of T , will be at order hT^2 to obtain a sparse version of $\hat{R}_{n,z}$. Linear interpolation is then used to estimate the components not computed. Therefore, the computation complexity in terms of T for $\hat{R}_{n,tq}$ can be reduced to hT^2 , and thus making our change point detection procedure applicable to high-dimensional functional data. If parallel computing is available, it can be utilized to start each off-diagonal's computation independently.

Based on our simulations, linear interpolation results in a negligible loss in power, and the size remains near the nominal level. Figure 1 illustrates $\hat{R}_{n,1,q}$ for all $q \in \{1, \dots, T-1\}$ and the corresponding interpolated values based on parameters $b = 20$ and $I = 8$. The fixed interval for off-diagonals was set to ten. The accuracy of the linear interpolation is evident under the null and alternative hypotheses. We apply the above computation strategies in simulation studies in Section 6 and compare the computation times before and after these improvements.

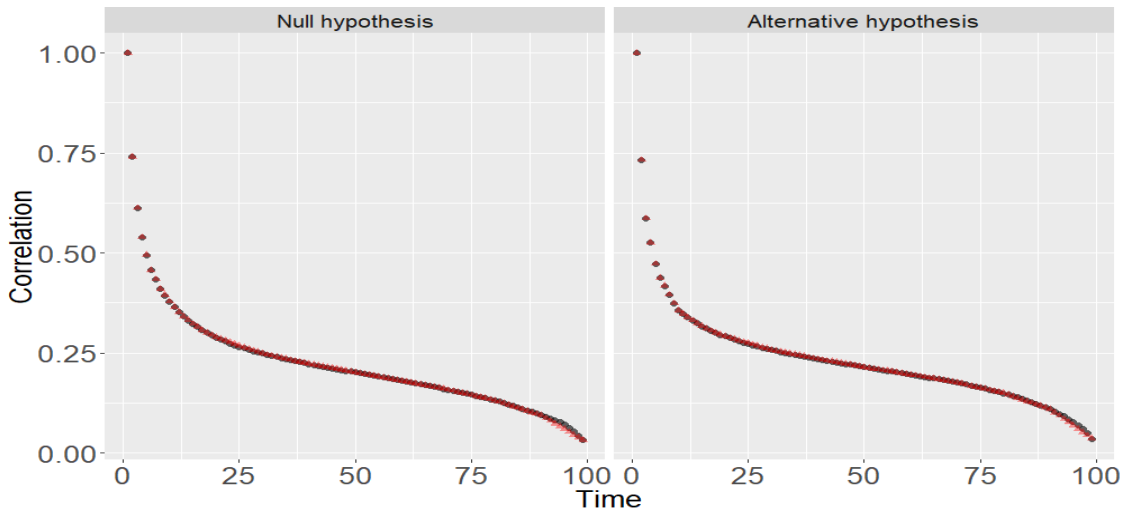


Figure 1: Accuracy of linear interpolation for $\hat{R}_{n,tq}$. Black circles represent $\hat{R}_{n,1q}$ for all $q \in \{1, \dots, T-1\}$. Red triangles represent the corresponding interpolated values.

5. Change point identification

If the data leads us to the conclusion to reject H_0 of (1), then a subsequent task is to identify the time points where changes exist among the T high-dimensional covariance matrices. We begin this discussion with only one change point under consideration. Let τ be the time point where a single change point exists, and consider the hypotheses

$$\begin{aligned} H_0 : \quad & \Sigma_1 = \cdots = \Sigma_T \quad \text{versus} \\ H_1^* : \quad & \Sigma_1 = \cdots = \Sigma_\tau \neq \Sigma_{\tau+1} = \cdots = \Sigma_T. \end{aligned} \quad (16)$$

Define $\hat{\tau}$ as an estimator for the change point's location, where

$$\hat{\tau} = \arg \max_{t \in \mathcal{T}} \hat{D}_{nt}, \quad (17)$$

and $\mathcal{T} = \{1, \dots, T-1\}$. The form of the estimator in (17) is motivated by the fact that D_t is maximized at time point $t = \tau$ when a single change point exists at time τ . The following theorem establishes the rate of convergence for $\hat{\tau}$.

Theorem 3. *Assume that H_1^* of (16) is true, and $\tau \asymp T^\delta$ for some $0 \leq \delta \leq 1$. Under C1 – C3, it follows that as $n \rightarrow \infty$,*

$$\hat{\tau}/\tau - 1 = O_p \left\{ \frac{\nu_{\max}}{\Delta_p} \frac{1}{\sqrt{n}} \frac{\sqrt{\log(T)}}{T^\delta} \right\},$$

where $\nu_{\max} = \max_{t \in \mathcal{T}} \max(\sqrt{V_{0t}/n}, \sqrt{V_{1t}})$, and $\Delta_p = \text{tr}\{(\Sigma_1 - \Sigma_T)^2\}$.

By Theorem 3, change point estimator, $\hat{\tau}$, is ratio-consistent provided that $\Delta_p/\nu_{\max} \gg T^{-\delta} \sqrt{\log(T)/n}$. Quantity Δ_p can be interpreted as the signal, and quantity ν_{\max} can be interpreted as the noise. Thus, if $\nu_{\max} \sqrt{\log(T)}/(\sqrt{n} \Delta_p T^\delta) \rightarrow 0$, $\hat{\tau}$ is a ratio-consistent estimator for τ . In most change point estimator studies the location of change point τ is assumed to be proportional to T . Theorem 3 permits a general setting, one that allows τ to reside on the boundary of the sequence since δ may be zero. Hence, the proposed change point estimator is consistent even on the boundaries provided the signal-to-noise ratio is adequate.

Based on the result in Theorem 3, the impact of data dimension and dependence, sample size and repeated measurements is reflected in quantities in ν_{\max}/Δ_p , $1/\sqrt{n}$ and $\sqrt{\log(T)}/T^\delta$,

respectively. Depending on the relationship between Δ_p and ν_{\max} , the data dimension and dependence can be a blessing or curse. It is a blessing if most dimensions contribute to the signal term, Δ_p , but do not inflate the noise, ν_{\max} , so much so that $\nu_{\max}/\Delta_p \rightarrow 0$. However, if an increased dimension and dependence add more noise than signal so that $\nu_{\max}/\Delta_p \rightarrow \infty$, then the high-dimensional dependent nature of the data has a negative effect.

Next we consider a general scenario with multiple change points as specified in H_1 of (1). There exist many procedures in the literature which extends a single change point identification procedure to multiple change points. Because of computation efficiency, we apply a commonly used procedure called binary segmentation (Vostrikova, 1981; Venkatraman, 1992) in this paper, but other procedures such as the wild binary segmentation (Fryzlewicz, 2014) can be also applied.

Let $\mathcal{Q} = \{1 \leq \tau_1 < \dots < \tau_q < T\}$ be the collection of all the q true change points, and let $\hat{\mathcal{Q}}$ be the estimated set of change points. For time points $t_1 < t_2$, let $S[t_1, t_2]$ be the quantity or statistic S based on data in time interval t_1 through t_2 . For example, $\nu_{\max}[t_1, t_2]$ is the quantity ν_{\max} defined on data within time interval $[t_1, t_2]$. The binary segmentation algorithm for multiple change points identification is detailed as follows.

Step 1: Compute \mathcal{M}_n and compare it with W_α . If $\mathcal{M}_n > W_\alpha$, then $\hat{\kappa} = \arg \max_{t \in \mathcal{T}} \hat{D}_{nt}$ is the estimated change point, and set $\hat{\kappa} = \hat{\tau}_1$ so $\hat{\mathcal{Q}} = \{\hat{\tau}_1\}$. Partition the full data set into two intervals: $[1, \hat{\kappa}]$ and $[\hat{\kappa} + 1, T]$ and proceed to step 2. However, if $\mathcal{M}_n \leq W_\alpha$, then no change points exist.

Step 2: Perform the detection procedure to test (1) using $Y[1, \hat{\kappa}]$ and $Y[\hat{\kappa} + 1, T]$. If H_0 is rejected based on $Y[1, \hat{\kappa}]$, then identify $\hat{\kappa}_1 = \arg \max_{t \in [1, \hat{\kappa}]} \hat{D}_{nt}[1, \hat{\kappa}]$ as a change point. Since $\hat{\kappa}_1 < \hat{\tau}_1$, set $\hat{\tau}_1 = \hat{\kappa}_1$ and $\hat{\tau}_2 = \hat{\kappa}$ so $\hat{\mathcal{Q}} = \{\hat{\tau}_1, \hat{\tau}_2\}$. Partition the data $Y[1, \hat{\kappa}]$ into two intervals: $[1, \hat{\kappa}_1]$ and $[\hat{\kappa}_1 + 1, \hat{\kappa}]$. If H_0 is not rejected, then no change points exist in the interval $[1, \hat{\kappa}]$. Repeat this procedure for the data based on interval $[\hat{\kappa} + 1, T]$. Set $\hat{\mathcal{Q}}$ is then updated to contain the ordered change points. If no change points are detected in either interval, then stop, as $\hat{\kappa}$ is the only change point that exists.

Step 3: If a change point is identified in at least one interval in step 2, repeat step 2 until no further change points are detected. At each step update and order set $\hat{\mathcal{Q}}$.

At the conclusion of the binary segmentation procedure we can partition the interval $[1, T]$ so each sub-interval will consist of end points from the set $\{1, \hat{Q}, T\}$. For example, if no change point is identified, then the single interval is $[1, T]$. If a single change point is identified at $\hat{\tau}$, then two intervals where no change points exist are $[1, \hat{\tau}]$ and $[\hat{\tau}, T]$. To establish the consistency of \hat{Q} we first define some interval notation. Let I_k be a time interval such that $I_k = [\tau_a + 1, \tau_b]$, where $a + 1 < b$ such that $a \in \{0, \dots, q - 1\}$ and $b \in \{2, \dots, q + 1\}$. Define $\tau_0 = 0$ and $\tau_{q+1} = T$. Thus, I_k is an interval with at least one change point. Assume the smallest maximum signal-to-noise ratio among all segments I_t is defined as $\min_{I_k} \max_{\tau_s \in I_k} \sigma_{n\tau_s, 0}^{-1}[I_k] D_{\tau_s}[I_k]$, and is denoted as mSNR.

Theorem 4. *Let $\delta_{\min, k} = \min_{\tau_k \in I_k} \delta_k$ for any interval I_k , and let \hat{q} be the number of identified change points. Assume that $\tau_k \asymp T^{\delta_k}$ for some $0 \leq \delta_k \leq 1$; as T diverges, $W_{\alpha_n} = o(\text{mSNR})$ and $\nu_{\max}[I_k] \sqrt{\log(T)} / (n \Delta_p[I_k] T^{\delta_{\min, k}}) \rightarrow 0$ for all intervals I_k . Therefore, under Conditions C1- C2, and C3, as $n \rightarrow \infty$ and $\alpha_n \rightarrow 0$, $\hat{q} \rightarrow q$ and, for all k , $\hat{\tau}_k / \tau_k \rightarrow 1$ in probability.*

In the existence of change points, the assumption that $W_{\alpha_n} = o(\text{mSNR})$ ensures the consistency of the proposed test at each phase of binary segmentation. In the absence of change points, the assumption that $\alpha_n \rightarrow 0$ ensures no change points will be detected and binary segmentation will stop on the current interval. The second assumption on the signal-to-noise ratio ensures that the change point estimator is ratio-consistent.

6. Simulation studies

In this section we present multiple simulation studies to demonstrate finite sample performance of the proposed change point detection and identification procedures in a large p , large T , and small n framework. In addition, we will also demonstrate the computation efficiency of our proposed algorithm.

6.1 Simulation settings

All data were generated from a multivariate linear process,

$$Y_{it} = \sum_{h=0}^L A_{t,h} \xi_{i(t-h)} \quad (i = 1, \dots, n; t = 1, \dots, T), \quad (18)$$

where $A_{t,h}$ is a $p \times p$ matrix, and $\xi_{i(t-h)}$ are p -dimensional multivariate normally distributed random vectors with mean 0 and covariance I_p . The data generation scheme given by (18) permits both spatial and temporal dependence. Spatial dependence occurs among the vector Y_{it} for a given time point t , and temporal dependence exists among $\{Y_{it}\}_{t=1}^T$ at different time points. By definition of Y_{it} in (18), $\text{cov}(Y_{it}, Y_{is}) = \sum_{h=t-s}^L A_{t,h} A_{s,h-(t-s)}^T I(t-s \leq L)$ if $t \geq s$. The spatial and temporal dependence is governed by the simulation parameter L .

For both change point detection and identification, we considered $n = 40, 50$ and 60 ; $p = 500, 750$ and 1000 ; and $T = 50$ and 100 . We considered an additional case with $T = 150$ for change point identification. Parameter L was set to be 3. Simulation results reported in Tables 1, 3 were based on 500 simulation replications, and simulation results in Table 2 were based on 100 simulation replications.

To evaluate the impact of dependence on the proposed procedures, we considered two structured types of matrices $A_{t,h}$ in order to control the spatial and temporal dependence. Exponential decay $A_{t,h}$ matrices were used for change point detection, and polynomial decay $A_{t,h}$ matrices were used for change point identification.

Define two matrices $B_1 = \{(0.6)^{|i-j|} I(|i-j| < p/5)\}$ and $B_2 = \{(0.6 + \delta)^{|i-j|} I(|i-j| < p/5)\}$, where (i, j) represents the i th row and j th column of the $p \times p$ matrices B_1 and B_2 . Let $\tau_1 = \lfloor T/2 \rfloor$ be the possible true underlying change point among the covariance matrices, where $\lfloor x \rfloor$ is the floor function. For all $h \in \{0, \dots, L\}$, define $A_{t,h} = B_1$ for $t \in \{1, \dots, \tau_1\}$, and $A_{t,h} = B_2$ for $t \in \{\tau_1 + 1, \dots, T\}$. Parameter δ in B_2 governs the signal strength in terms of how different the covariance matrices are before and after the change point at time τ_1 . When $\delta = 0$, then $B_1 = B_2$ and matrices $A_{t,h}$ are the same for all t ; thus there is no change point among covariance matrices, and the null hypothesis is true. If $\delta > 0$, then the null hypothesis is false, and τ_1 is the true covariance change point. For the change point detection simulation results in Table 1, δ was set to 0.00, 0.025, 0.05 and 0.10.

To evaluate the performance of the change point identification procedure and the proposed binary segmentation procedure, consider two change points: τ_1 and τ_2 . Let $\tau_1 = \lfloor T/2 \rfloor$, and let $\tau_2 = \tau_1 + 2$. Define three matrices, $B_1^* = \{(|i-j| + 1)^{-2} I(|i-j| < p/5)\}$, $B_2^* = \{(|i-j| + \delta^* + 1)^{-2} I(|i-j| < p/5)\}$, and $B_3^* = \{(|i-j| + 2\delta^* + 1)^{-2} I(|i-j| < p/5)\}$, where (i, j) represents the i th row and j th column of the $p \times p$ matrices B_1^* , B_2^* , and B_3^* .

Thus, for $h \in \{0, \dots, 3\}$, $A_{t,h} = B_1^*$ for $t \in \{1, \dots, \tau_1\}$, $A_{t,h} = B_2^*$ for $t \in \{\tau_1 + 1, \dots, \tau_2\}$ and $A_{t,h}^* = B_3^*$ for $t \in \{\tau_2 + 1, \dots, T\}$. Since our purpose is to demonstrate the finite sample accuracy of change point identification, we chose values of δ to be 0.15, 0.25, and 0.35.

Two measures were considered to evaluate the change point identification procedure's efficacy: average true positives and average true negatives. For each simulation replication there exists two true change points at time points τ_1 and τ_2 , and there exists $T - 3$ time points where no change point exists. The average true positives are defined as the average number of correctly identified change points among 100 simulation replications. Similarly, the average true negatives are defined as the average number of correctly identified time points where no covariance change exists among 100 simulation replications.

6.2 Simulation results with exactly computed quantiles

Table 1 demonstrates the empirical size and power of the proposed test procedure at nominal level 5%. The quantiles were obtained from the zero-mean multivariate Gaussian process, where every element of correlation matrix $\hat{R}_{n,tq}$ was computed exactly. We observe that the empirical size is well controlled for all combinations of n , p , and T . For a fixed p and T , as n increases the power increases. Likewise, as δ increases, the power of the change point detection procedure increases. For a fixed n and p , the power also increases as T increases.

Table 2 provides the average true positives and average true negatives along with their corresponding standard errors of the proposed identification and binary segmentation procedure in the large p , large T , and small n setting. For fixed p , n , and T , the average true positives and average true negatives approach their true values two and $T - 3$, respectively, as δ increases. As the sample size increases, the average true positives and average true negatives approach their maximal values. Our results indicate that the proposed methods work well under various scenarios and are consistent in locating change points when the signal-to-noise ratio is increased.

Table 1: Empirical size and power of the proposed change point detection test. The numbers in the table are percentages of simulation replications that reject the null hypothesis at nominal level 5%.

δ	n/p	$T = 50$			$T = 100$		
		500	750	1000	500	750	1000
0 (size)	40	4.4	4.6	3.8	3.6	5.4	4.4
	50	4.8	4.0	3.6	2.0	4.6	4.0
	60	3.8	4.2	2.8	5.4	3.6	5.6
0.025	40	13.4	13.4	10.8	18.0	19.0	18.0
	50	17.0	19.2	17.0	30.6	27.2	30.4
	60	26.4	26.0	27.4	47.0	41.6	41.6
0.05	40	96.0	97.0	98.0	100	100	100
	50	100	100	100	100	100	100
	60	100	100	100	100	100	100
0.10	40	100	100	100	100	100	100
	50	100	100	100	100	100	100
	60	100	100	100	100	100	100

Table 2: Average true positives (ATP) and average true negatives (ATN) for identifying multiple change points using the proposed binary segmentation method. The standard errors of ATP and ATN are included in the parentheses.

T	p	n	$\delta=0.15$		$\delta=0.25$		$\delta=0.35$	
			ATP	ATN	ATP	ATN	ATP	ATN
50	500	40	1.20 (0.40)	46.76 (0.62)	1.68 (0.47)	46.48 (0.52)	1.97 (0.17)	46.62 (0.49)
		50	1.41 (0.49)	46.68 (0.53)	1.91 (0.29)	46.42 (0.52)	2.00 (0.00)	46.63 (0.49)
		60	1.57 (0.50)	46.58 (0.55)	1.98 (0.14)	46.52 (0.50)	2.00 (0.00)	46.61 (0.55)
	750	40	1.30 (0.46)	46.78 (0.42)	1.77 (0.42)	46.51 (0.50)	2.00 (0.00)	46.59 (0.61)
		50	1.33 (0.47)	46.66 (0.48)	1.95 (0.22)	46.53 (0.50)	2.00 (0.00)	46.70 (0.46)
		60	1.57 (0.50)	46.58 (0.55)	1.99 (0.10)	46.53 (0.56)	2.00 (0.00)	46.64 (0.50)
	1000	40	1.27 (0.45)	46.76 (0.55)	1.81 (0.39)	46.61 (0.51)	1.95 (0.22)	46.59 (0.50)
		50	1.48 (0.50)	46.67 (0.47)	1.95 (0.22)	46.58 (0.50)	2.00 (0.00)	46.76 (0.43)
		60	1.65 (0.48)	46.51 (0.63)	1.99 (0.10)	46.69 (0.47)	2.00 (0.00)	46.59 (0.67)
100	500	40	1.27 (0.45)	96.75 (0.50)	1.74 (0.44)	96.56 (0.50)	1.98 (0.14)	96.54 (0.52)
		50	1.31 (0.47)	96.67 (0.47)	1.92 (0.27)	96.54 (0.50)	2.00 (0.00)	96.44 (0.50)
		60	1.62 (0.49)	96.70 (0.48)	1.99 (0.10)	96.56 (0.52)	2.00 (0.00)	96.46 (0.54)
	750	40	1.22 (0.42)	96.76 (0.50)	1.85 (0.36)	96.59 (0.51)	1.98 (0.14)	96.54 (0.50)
		50	1.33 (0.47)	96.59 (0.55)	1.96 (0.20)	96.51 (0.50)	2.00 (0.00)	96.54 (0.50)
		60	1.60 (0.49)	96.59 (0.49)	1.99 (0.10)	96.55 (0.50)	2.00 (0.00)	96.42 (0.78)
	1000	40	1.20 (0.40)	96.80 (0.43)	1.74 (0.44)	96.52 (0.50)	1.98 (0.14)	96.59 (0.55)
		50	1.34 (0.48)	96.64 (0.50)	1.90 (0.30)	96.50 (0.52)	2.00 (0.00)	96.49 (0.50)
		60	1.59 (0.49)	96.50 (0.61)	2.00 (0.00)	96.58 (0.50)	2.00 (0.00)	96.44 (0.61)
150	500	40	1.19 (0.39)	146.76 (0.43)	1.73 (0.45)	146.53 (0.56)	1.97 (0.17)	146.48 (0.56)
		50	1.34 (0.48)	146.68 (0.47)	1.95 (0.22)	146.55 (0.50)	2.00 (0.00)	146.40 (0.53)
		60	1.54 (0.50)	146.51 (0.52)	2.00 (0.00)	146.57 (0.50)	2.00 (0.00)	146.53 (0.52)
	750	40	1.16 (0.37)	146.84 (0.40)	1.73 (0.45)	146.58 (0.50)	1.97 (0.17)	146.46 (0.58)
		50	1.42 (0.50)	146.64 (0.50)	1.97 (0.17)	146.55 (0.52)	2.00 (0.00)	146.52 (0.56)
		60	1.56 (0.50)	146.45 (0.58)	1.98 (0.14)	146.42 (0.52)	2.00 (0.00)	146.55 (0.56)
	1000	40	1.20 (0.40)	146.80 (0.40)	1.72 (0.45)	146.49 (0.50)	1.97 (0.18)	146.51 (0.52)
		50	1.46 (0.50)	146.70 (0.46)	1.92 (0.27)	146.50 (0.67)	2.00 (0.00)	146.47 (0.63)
		60	1.53 (0.50)	146.56 (0.54)	1.99 (0.10)	146.56 (0.52)	2.00 (0.00)	146.51 (0.50)

6.3 Approximation algorithm and improved computation time

To illustrate the accuracy of the proposed approximation algorithm in Section 4, Table 3 conveys the empirical size and power of the proposed test procedure. Rather than compute $\hat{R}_{n,tq}$ for all $t, q \in \{1, \dots, T-1\}$, we computed the first b off-diagonals and the last w columns of $\hat{R}_{n,tq}$. The remaining values were imputed via linear interpolation. In the simulation studies, parameter $b = 5$, and $w = 5, 10$ and 20 . We observe that the sizes of the test based on the approximated quantiles are well maintained at the nominal level of 0.05 , and there are minuscule differences from the empirical sizes in Table 1. Furthermore, there is only a minimal difference in power when compared to the corresponding results in Table 1. These results indicate the proposed approximation maintains accuracy. The simulation results for cases when $b = 10$ and 20 are included in the supplementary files.

Table 3: Empirical size and power of the proposed test for $T = 100$, percentages of simulation replications that reject the null hypothesis, quantile computed from a correlation matrix that used proposed approximation in Section 4. The first 5 off-diagonals were computed exactly as well as the last w components for each row

δ	n/p	$w = 5$			$w = 10$			$w = 20$		
		500	750	1000	500	750	1000	500	750	1000
0(size)	40	3.4	4.8	4.2	3.4	4.8	4.2	3.4	5.2	4.2
	50	2.0	4.6	3.8	2.0	4.6	4.0	2.0	4.6	4.0
	60	4.8	3.2	5.0	4.8	3.2	5.0	5.2	3.8	5.6
0.025	40	17.8	19.0	17.6	17.8	19.0	17.6	17.8	19.0	17.6
	50	30.8	26.2	30.2	30.8	26.6	30.2	30.8	26.6	30.2
	60	46.6	40.8	41.0	46.6	40.8	41.0	46.6	41.2	41.0
0.050	40	100	100	100	100	100	100	100	100	100
	50	100	100	100	100	100	100	100	100	100
	60	100	100	100	100	100	100	100	100	100
0.100	40	100	100	100	100	100	100	100	100	100
	50	100	100	100	100	100	100	100	100	100
	60	100	100	100	100	100	100	100	100	100

Applying expressions (11) – (14) we evaluate and compare the computation time with

that of the naive detection method. Our algorithm improves the computation efficiency with respect to the sample size n and the number of repeated measurements T . To see the improvements, we isolate these two parameters and consider two cases. In the first case, we consider $p = 1, n = 4$ and $T = 50, 75, 100, 125, 150$ so so we can quantify the affect of reducing the computation complexity with respect to T . In the second case, we consider $p = 1, T = 2$ and $n = 30, 60, 90, 120, 150$ so that we can evaluate the saved computation time with respect to n . Figure 2 compares the median computation time of the naive method and the proposed method using expressions (11) – (14). Each parameter combination was run for 100 simulation replications. The left plot illustrates the computation time in seconds as T varies for each method. When $T = 150, n = 4$ and $p = 1$, the naive method had a median run time of 36830.685 seconds; while for the same data and parameter combinations the proposed method had a median run time of 429.898 seconds. This is equivalent to 10.23 hours versus 7.16 minutes. Similarly, the right plot illustrates the computation time in seconds as n varies for each method. For $n = 150, T = 2$ and $p = 1$ the median run time of the proposed method is over 266 times faster than the median run time of the naive method.

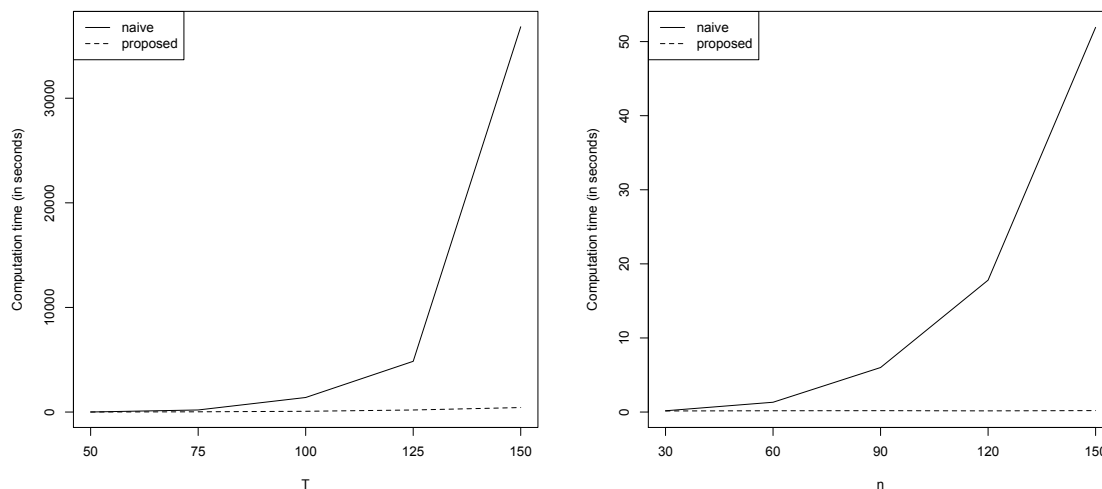


Figure 2: Computation time of the naive method and proposed computation method in Section 4. The left panel is the comparison with respect to T while the right panel is with respect to n .

7. An application to event segmentation

Event segmentation theory (Zacks et al., 2007) suggests that humans generate event boundaries in memory by partitioning a continuous experience into a series of segmented discrete events. Schapiro et al. (2013) discovered that event boundaries are formed around changes in functional connectivity. In this section we apply our proposed procedure to detect and identify change points in covariance matrices in the fMRI data set collected by Chen et al. (2017) to partition fMRI data into a series of segments with static functional connectivity within each segment. Time points where functional connectivity changes may represent event boundaries as suggested in the aforementioned neuroscience literature.

We apply our proposed method to the motivating task-based fMRI experiment (Chen et al., 2017) introduced in Section 1. The experiment involved 17 participants that each watched the same 48-minute segment (episode 1: “a study of pink”) of the BBC television series *Sherlock* while undergoing an fMRI scan. None of the participants had watched the series *Sherlock* prior to the study. A 30-second cartoon was prepended to the movie to allow the brain time to adjust to new audio and visual stimuli. Including an unrelated cartoon prior to studies such as this is common practice as it reduces statistical noise. Subjects were instructed to watch the television episode as they would watch a typical television episode in their own home. Data were gathered from a Siemens Skyra 3T full-body scanner, and the fMRI machine acquired an image of each participant’s brain every 1.5 seconds. As a result, the 48-minute segment of *Sherlock* resulted in 1,976 repeated measurements. More details about the experiment and processes of acquiring functional and anatomical images are provided in Chen et al. (2017).

To demonstrate our proposed methods, we analyzed the first 131 time points of fMRI data which corresponds to the preface of *Sherlock*, or equivalently the first three minutes and 16 seconds of the movie. Let Y_{it} ($i = 1, \dots, 17$; $t = 1, \dots, 131$) be the 268-dimensional random vector containing the BOLD measurements for the 268 nodes of the i th individual at time t . A node, or region of interest, represents a collection of voxels. The 268 node parcellation was performed according to Shen et al. (2013), where voxel groupings ensure functional homogeneity within each node, making it ideal for node network and dynamic

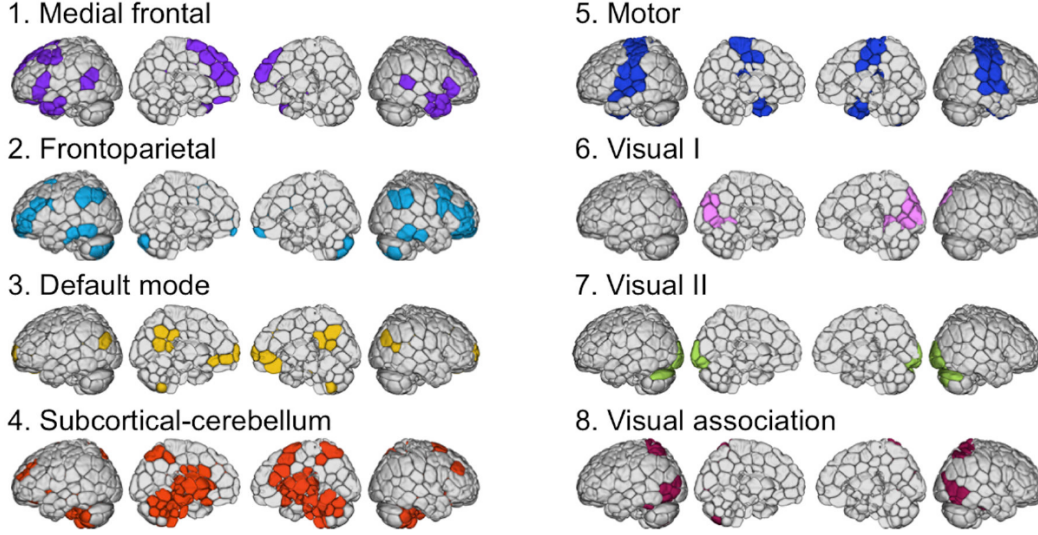


Figure 3: 268 Shen-node parcellation. This image was obtained from Finn et al. (2015).

functional connectivity analysis. Figure 3 illustrates the 268 Shen node parcellation along with large-scale node groupings. A node-level analysis, as opposed to a voxel-level analysis, allows for more interpretable results. For further details on the benefits and processes of Shen node parcellation, we refer readers to Shen et al. (2013). In summary, the fMRI data contains $p = 268$ random variables that are repeatedly measured for $T = 131$ times from $n = 17$ subjects.

Let Σ_t be the covariance matrix of Y_{it} ($t = 1, \dots, 131$). Matrix Σ_t , or its inverse, is a 268×268 -dim matrix that represents the functional connectivity among 268 nodes at time t . The goal of our analysis is to detect if there is any changes among Σ_t 's. If change point exists, we further identify the locations of the change points, which will be applied to partition the movie preface into discrete event segments. We first applied our test procedure proposed in Section 3 and obtained the test statistic value $\mathcal{M}_n = 4.433$; we rejected H_0 of (1) as the p-value was less than 0.001. This result suggests that the functional connectivity among the 268 nodes changes over time. Accordingly, we applied the proposed binary segmentation to identify all significant change points among 131 covariance matrices. Our proposed method identified 20 change points at time points 2, 25, 36, 39, 40, 41, 42, 58, 60, 61, 63, 81, 83, 110, 113, 114, 115, 116, 128 and 130. Based on the identified change points, we observe that several clusters exist. The first cluster occurred at 39, 40, 41 and 42, the second cluster

occurred at 58, 60, 61 and 63, the third cluster occurred at 81 and 83, and the last cluster appeared at 110, 113, 114, 115 and 116. This phenomena indicates that the functional connectivity changes slowly, rather than abruptly, around these change points, and different individuals may have slightly different points of change due to individual heterogeneity.

To use these change points for event segmentation, we group the sets of change points that are close to each other because these sets of change points essentially imply the same event boundaries. After grouping, the change points used for event segmentation are 2, 25, 36, 42, 58, 83, 113 and 130, where 42, 58, 83 and 113 are representations of their respective group of event boundaries. Change points 2 and 130 coincide with the beginning of the stimuli and the end of preface. Therefore, change points 25, 36, 42, 58, 83 and 113 are used for event segmentation, which corresponds to 38, 54, 63, 87, 125 and 170 seconds in the movie.

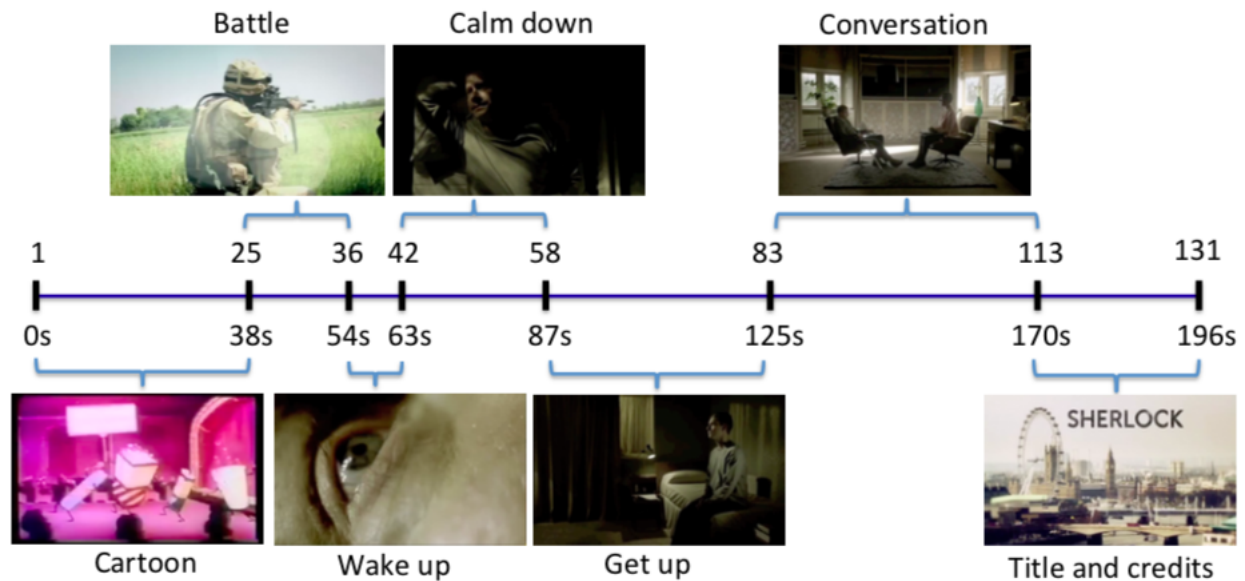


Figure 4: Event segmentation based on the covariance change points in fMRI data detected and identified by using the proposed approaches. Images were obtained from the movie *Sherlock*.

Figure 4 illustrates the final event segmentation using the proposed approach and the corresponding events in each segment. The event partitions based on the identified change points coincide with important situations in the television episode *Sherlock*. The first segment

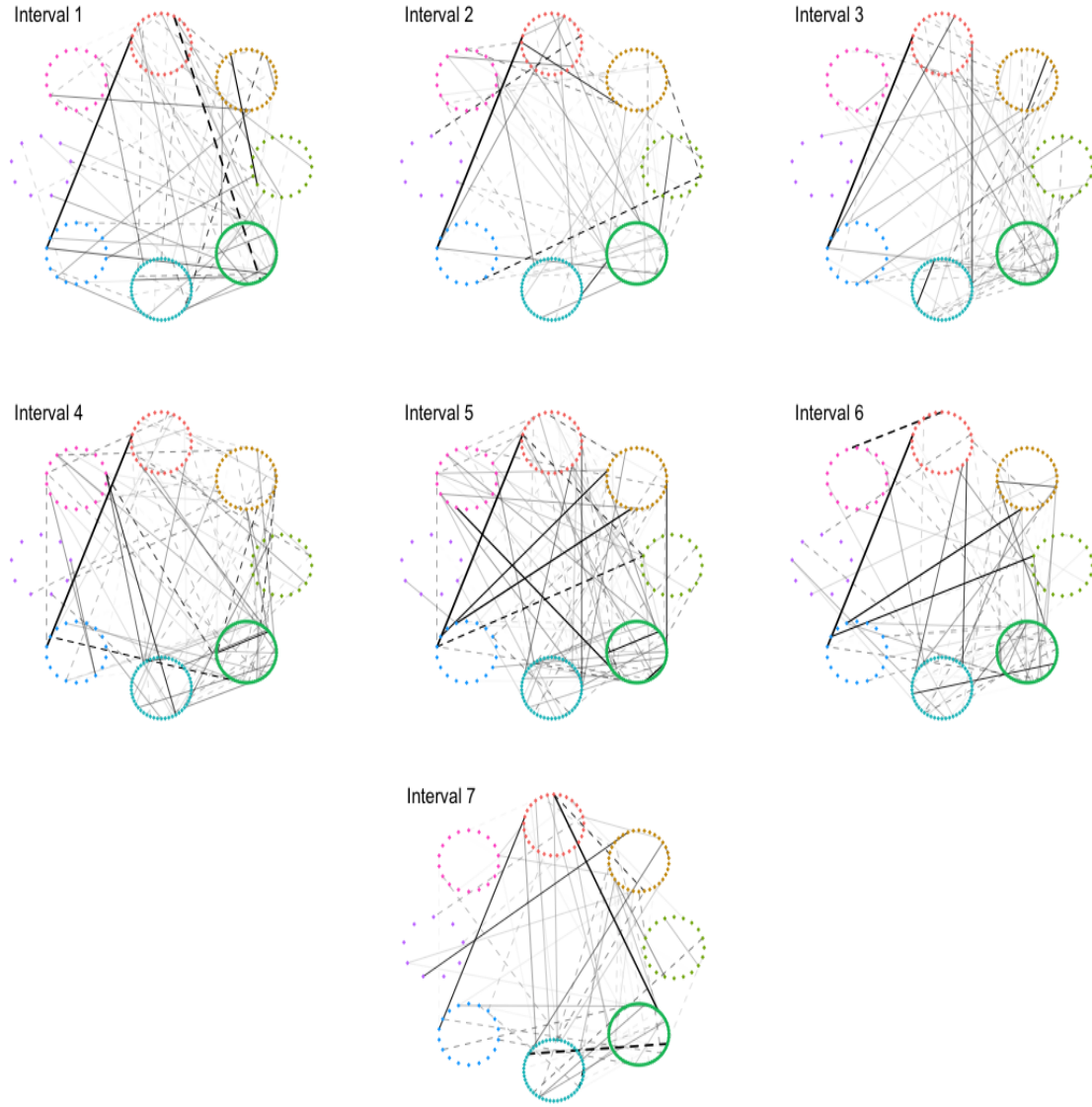


Figure 5: Correlation networks based on an average over a time interval in which the covariance matrices are homogeneous. Each circle is comprised of 67 Shen nodes. Solid lines represent a positive correlation, and dashed lines represent a negative correlation. The darker the line the stronger the correlation between nodes. A correlation threshold value of 0.70 in absolute values was used.

is from the beginning to the first change point (38s in the movie), which corresponds to the cartoon “let us all go to the lobby” prepended to the movie. The second segment, between 38s and 54s, in the movie corresponds to flashbacks of battle scenes. The third segment, between 54s and 63s, corresponds to the period of Watson, the main character, awakening from his dream. The fourth segment, between 63s and 87s, is a period where Watson calms down. Between 87 and 125 seconds is the period that Watson got up and prepared to write his blog. During the sixth segment, between 125s and 170s, Watson is having a conversation with a journalist. The final segment, from 170s to the end of the preface, corresponds to the title and introductory credits.

Figure 5 demonstrates the changes in covariance matrices around the change points used in Figure 4. Each subplot is the estimated correlation matrix between nodes using the data between change points. For example, in Figure 5, the correlation network in interval 1 is estimated based fMRI data between time interval [3, 25]. We observe that the correlation networks estimated from different intervals are significantly different from each other. This indicates that the identified change points are consistent with the changes in correlation networks. Correlation network layouts are structured according to the eight large-scale node groupings illustrated in Figure 3. The top-centered circle consists of nodes within the medial frontal group. Moving clockwise on a given sub-plot, the remaining circles represent frontoparietal, default mode, subcortical-cerebellum, motor, visual I, visual II, and visual association.

References

- Anderson, T. W. (2003), *An Introduction to Multivariate Statistical Analysis*, New York: John Wiley.
- Barnett, I and Onnela, J.-P. (2016). Change point detection in correlation networks, *Scientific Report* **6**, 18893.
- Bickel, P. and Levina, E. (2008), “Regularized estimation of large covariance matrices,” *Annals of Statistics*, 36, 199–227.

- Chen, J., Leong, Y., Honey, C., Yong, C., Norman, K., and Hasson, U. (2017), “Shared memories reveal shared structure in neural activity across individuals,” *Nature Neuroscience*, 20(1), 115–125.
- Chiou, J.-M., Chen, Y.-T. and Yang, Y.-F. (2014), “Multivariate functional component analysis: A normalization approach,” *Statistica Sinica*, 24, 1571–1596.
- Cribben, I., Wager, T. D. and Lindquist, M. A. (2013). “Detecting functional connectivity change points for single-subject fMRI data,” *Frontiers in computational neuroscience*, 7, 143.
- Dette, H., Pan, G., and Yang, Q. (2018), “Estimating a change point in a sequence of very high-dimensional covariance matrices,” *arXiv:1807.10797*.
- Dehling, H., Fried, R., Garcia, I. and Wendler, M. (2013), “Change-point detection under dependence based on two-sample U-statistics,” *Asymptotic methods in stochastics: Festschrift in honor of Miklos Csörgő’s 80th birthday*.
- Finn, E. S., Shen, X., Scheinost, D., Rosenberg, M. D., Huang, J., Chun, M. M., Papademetris, X., and Constable, R. T. (2015), “Functional connectome fingerprinting: identifying individuals using patterns of brain connectivity,” *Nature Neuroscience*, 18(11), 1664–1671.
- Fryzlewicz, P. (2014), “Wild binary segmentation for multiple change-point detection.” *The Annals of Statistics*, 42, 2243–2281.
- Hall, P., Müller, H.-G., and Wang, J.-L. (2006). “Properties of principal component methods for functional and longitudinal data analysis.” *Annals of Statistics*, 34, 1493–1517.
- Horváth, L. and Kokoszka, P. (2012), *Inference for functional data with applications*, New York: Springer.
- Ishii, A., Yata, K. and Aoshima, M. (2016). “Asymptotic properties of the first principal component and equality tests of covariance matrices in high-dimension, low-sample-size context.” *Journal of Statistical Planning and Inference*, 170, 186–199.

- Ishii, A., Yata, K., and Aoshima, M. (2019). “Equality tests of high-dimensional covariance matrices under the strongly spiked eigenvalue model” *Journal of Statistical Planning and Inference*, 202, 99-111.
- Jung, Sungkyu and Marron, J. S. (2009), “PCA consistency in high dimension, low sample size context.” *Annals of Statistics*, 37, 4104–4130.
- Kundu, S., Ming, J., Pierce, J., McDowell, J., and Guo, Y. (2018), “Estimating dynamic brain functional networks using multi-subject fMRI data,” *Neuroimage*, 183, 635–649.
- Li, J. and Chen, S. X. (2012), “Two sample tests for high-dimensional covariance matrices”. *Annals of Statistics*,” 40, 908–940.
- Li, Y. and Hsing, T. (2010), “Uniform convergence rates for nonparametric regression and principal component analysis in functional/longitudinal data”. *Annals of Statistics*,” 38, 3321–3351.
- Monti, R., Hellyer, P., Sharp, D., Leech, R., Anagnostopoulos, C., and Montana, G. (2014), “Estimating time-varying brain connectivity networks from functional MRI time series,” *Neuroimage*, 103, 427–443.
- Muirhead, R. J. (2005), *Aspects of Multivariate Statistical Theory*, New York: John Wiley.
- Pourahmadi, M. (2013), *High-dimensional covariance estimation*, New York: John Wiley.
- Schapiro, A., Rogers, T., Cordova, N., Turk-Browne, N., and Botvinick, M. (2013), “Neural representations of events arise from temporal community structure,” *Nature Neuroscience*, 16(4), 486–492.
- Schott, J. (2007), “A test for the equality of covariance matrices when the dimension is large relative to the sample size,” *Computational Statistics and Data Analysis*, 51, 6535–6542.
- Shen, X., Tokoglu, F., Papademetris, X., and Constable, R. (2013), “Groupwise whole-brain parcellation from resting-state fMRI data for network node identification,” *Neuroimage*, 82, 403–415.

- Srivastava, M. S., and Yanagihara, H. (2010), “Testing the equality of several covariance matrices with fewer observations than the dimension,” *Journal of Multivariate Analysis*, 101, 1319–1329.
- Venkatraman, E. S. (1992), “Consistency results in multiple change-point situations,” *Technical report*, Department of Statistics, Stanford University.
- Vostrikova, L. (1981). “Detecting disorder in multidimensional random processes,” *Soviet Mathematics Doklady*, 24, 55–59.
- Wang, D., Yu, Y., and Rinaldo, A. (2017), “Optimal Covariance Change Point Localization in High Dimension,” *arXiv:1712.09912*
- Xiao, L., Zipunnikov, V., Ruppert, D., and Crainiceanu, C. (2016). Fast Covariance Estimation for High-dimensional Functional Data. *Statistics and computing*, 26, 409–421.
- Zacks, J., Speer, N., Swallow, K., Braver, T., and Reynolds, J. (2007), “Event perception: A mind-brain perspective,” *Psychological Bulletin*, 133(2), 273–293.
- Zalesky, A., Fornito, A., Cocchi, L., Gollo, L. L. and Breakspear, M. (2014). “Time-resolved resting-state brain networks.” *Proc. Natl. Acad. Sci.*, 111, 10341–10346.
- Zhang, C., Bai, Z., Hu, J., and Wang, C. (2018), “Multi-sample test for high-dimensional covariance matrices,” *Communications in Statistics - Theory and Methods*, 47:13, 3161–3177.
- Zhong, P.-S., Li, R. and Santo, S. (2019), “Homogeneity tests of covariance matrices with high-dimensional longitudinal data,” *Biometrika*, 106:3, 619–634.